Self-Organization of Local Cortical Circuits and Cortical Orientation Maps: A Nonlinear Hebbian Model of the Visual Cortex with Adaptive Lateral Couplings

Thomas Burger[§] and Elmar Wolfgang Lang*

Institute of Biophysics, Universität Regensburg, D-93040 Regensburg, Germany.
E-mail: elmar.lang@biologie.uni-regensburg.de

* Author for correspondence and reprint requests

Z. Naturforsch. **56c,** 464–478 (2001); received August 11, 2000/February 1, 2001

Self-Organisation, Local Cortical Circuits, Nonlinear Hebbian Learning

A nonlinear, recurrent neural network model of the visual cortex is presented. Orientation maps emerge from adaptable afferent as well as plastic local intracortical circuits driven by random input stimuli. Lateral coupling structures self-organize into DOG profiles under the influence of pronounced emerging cortical activity blobs. The model's simplified architecture and features are modeled to largely mimik neurobiological findings.

Introduction

The primary visual cortex of mammals is well investigated and its functional architecture is known in considerable detail now (Hubel and Wiesel, 1977) (Lund *et al.*, 1994). In early stages of visual information processing simple features are extracted mainly from visual stimuli. Most cortical neurons within V1 respond selectively to oriented contrast contours (edges and bars) in the visual input. The receptive fields of such simple cells are segregated into elongated subfields of alternating response to small spot light stimuli (Jones and Palmer, 1987). These cortical simple cells with varying orientation specificity are grouped laterally into piecewise continous orientation preference and selectivity maps along the cortical surface. These maps are characterized by $\pm 1/2$-vortices, where the orientation preferences change by $\pm 180°$ along a closed path around the vortex center (Blasdel, 1992) (Bonhoeffer and Grinvald, 1991). Furthermore iso-orientation domains exist, where all cells have similar orientation preferences as well as linear zones and fractures where orientation varies smoothly or abruptly, respectively.

Another feature which cortical simple cells encode is ocular dominance which relates to the observation that many neurons respond preferably to input from one eye only. Cortical cells which prefer the input by the same eye form ocular dominance stripes in monkey cortex (Le Vay *et al.*, 1975) or group into patches in cat cortex (Le Vay *et al.*, 1978).

Though the functional architecture is well characterized experimentally the mechanisms by which these feature detectors group together laterally in an activity dependent manner into cortical feature maps during prenatal and early postnatal development is still not well understood. Especially the role of neural activity during the self-organization of orientation maps is still in disput (Weliky and Katz, 1997; Crair *et al.*, 1998).

These discoveries have since prompted the design of computational models for the investigation of possible mechanisms controlling the development of cortical feature maps (Swindale, 1996). Inspired by the seminal papers of von der Malsburg (1973) and Linsker (1986) Miller presented a rather advanced correlation-based Hebbian learning (CBL) model (Miller, 1994) for the development of simple cell receptive field structures and the emergence of orientation maps. He used a multilayer neural network using a linear Hebbian learning rule with subtractive constraints and synapse clipping. This rule considers artificial input activity correlation functions instead of real input patterns. Further his model was monocular only, but two LGN layers (ON- and OFF-center LGN cells) were implemented. Miller achieved segregated orientation selective receptive fields and orientation maps containing $\pm 1/2$ vortices. The intra-

[§] Financial support by the Friedrich-Ebert-Stiftung and the DFG is gratefully acknowledged.

0939–5075/2001/0500–0464 $ 06.00

cortical lateral interaction structure was static and modelled by either an excitatory Gaussian profile or a difference of Gaussians (DOG) profile with short-range excitation and longer-range inhibition. Biasing the coupling structure this way may be justified by neurobiological investigations of local circuits in cortex (Fisken *et al.*, 1973).

A similar monocular CBL model of orientation map formation was independently developed by Stetter *et al.* (1994), too. This model led to orientation selective bilobed receptive fields and orientation maps. Again a static spatially oscillating intracortical interaction was implemented, inter alia formed as a DOG profile to organize the formation of the feature map. The latter, however contained ± 1 vortices instead of experimentally observed ± 1/2 vortices. Within a binocular version of the model (Stetter *et al.*, 1995) the emergence of ocular dominance structures could be investigated also. But ocular dominance patches did emerge only in case of unbalanced ON/OFF-ganglion cell responses in their model much like in the earlier Miller model (Miller *et al.*, 1989). Indeed Piepenbrock (1996b) recently showed that the formation of both orientation and ocular dominance maps decouple in linear CBL models and suggested a two step process.

Another rather advanced model of orientation selectivity was introduced by Somers *et al.*, (1995). His monocular network model of spiking neurons used oriented flashed bar stimuli as input. The receptived fields of the ON- and OFF-center ganglion cells were represented as two-dimensional Gaussians with a common space constant for both dimensions. The ganglion cell activity was restricted to non-negative values. These activity values were used to generate spikes in LGN neurons using a Poisson process. Cortical cells received input from LGN neurons, cortical excitatory, and cortical inhibitory neurons with fixed intracortical synaptic couplings. Somer's model concentrated on the emergence of orientation selectivity of single cells and did not investigate the development of orientation maps.

Almost all previous neural network models did not use modifiable intracortical couplings. This seems an essential drawback as experimental findings (Callaway and Katz, 1990; Katz *et al.*, 1989; Katz and Callaway, 1992) point to a rather substantial plasticity of lateral interactions in visual cortex of monkeys and cats (Gilbert and Wiesel, 1989; Gilbert *et al.*, 1990). Hence, the implementation of cortical plasticity is essential to understand how plastic lateral interactions may affect the developing structures of cortical receptive fields and feature maps.

Sirosh and Miikkulainen (1994) presented their so-called LISSOM (laterally interconnected synergetically self-organizing map) model, which represents an extension of competitive self-organizing map (SOM) models (Sirosh and Miikkulainen, 1997). They implemented Gaussian spots on the retina as input signals for the cortical cells. Also a piecewise linear approximation to a sigmoidal activation function was used and only the ON-pathway was considered, hence no OFF cells existed. With this model, only non-orientation selective receptive fields emerged. But in contrast to the models decribed above, plastic lateral connections were realized. There was a short-range excitation and a longer-range inhibition. This lateral coupling profile was organized into a DOG or Mexican hat profile, respectively.

Recently we proposed an incremental Hebbian learning model with modifiable intracortical couplings (Burger *et al.*, 1997a; Burger and Lang, 1997b; Burger and Lang, 1999). This linear neural network model yielded realistic orientation maps and spatially oscillating, mexican-hat-like lateral connection structures, on average, whenever the excitatory lateral couplings were confined to a shorter range than the inhibitory couplings around any given cortical neuron.

None of these models thus seems to incorporate all essential features into one single neural network model. Therefore we present an improved, nonlinear incremental binocular Hebbian learning model with real stimuli presented to the input layer, separate ON- and OFF-pathways with inter-LGN couplings and a sigmoidal activation function and lateral plasticity in the output layer (Burger 1999). We will show that the model leads to orientation selective cortical cells which are organized into realistic orientation maps. As a response to input stimuli activity blobs form in the output layer and spatially oscillating, mexican-hat-like lateral coupling profiles emerge even from unbiased initial lateral coupling structures.

The model

The binocular multilayer network model possesses two retinal input layers (left/right), four ganglion cell/LGN layers (left/right, ON/OFF) and a cortex layer (Fig. 1). Each of the layers forms a regular square lattice with a neuron per node. Each cell has a localized receptive field, which is centered on an retinotopically corresponding site of the preceding layer. The cells in the cortical layer may correspond to cortical simple cells.

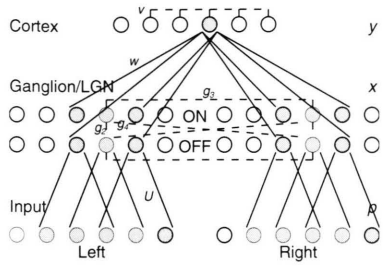

Fig. 1. The architecture of the network model. See text for details.

The layers

The retinal layers

The activites (denoted as $p(\vec{r}_p)$, where $\vec{r}_p$ describes the location of a special cell) of the retinal input layer neurons are confined to non-negative random values within the interval [0.0, 1.0]. This may represent a prenatal situation, where spontaneous uncorrelated activities were found by several investigators (Braitenberg and Schütz, 1991). Recently correlated retinal ganglion cell activity waves (Meister *et al.*, 1991; Wong and Oakley, 1996; Wong, 1999) have been described. But these stimulus patterns are probably too large in their characteristic wave length to be able to drive the development of orientation selectivity in cortical simple neurons (Miller, 1994). Furthermore it has been shown that artificially correlated activity patterns do not interfere with these retinal waves in blocking normal development of orientation specificity (Weliky and Katz, 1997). Therefore these patterned retinal waves have not been considered as relevant input stimuli in this investigation.

The receptive fields $U^{\alpha,\beta}(\vec{r}_x, \vec{r}_p)$ of the ganglion cells are DOG shaped and possess a center-surround antagonism. In case of an ON-ganglion cell this reads

$$U^{\alpha,on}(\vec{r}_x, \vec{r}_p) = U^{\alpha,\mathrm{on}}(\vec{r}_p - \vec{r}_x) \tag{1}$$

$$= N_U \cdot \left(\exp\left(-\frac{|\vec{r}_p - \vec{r}_x|^2}{r_U^2}\right) - \frac{1}{\alpha_U^2} \exp\left(-\frac{|\vec{r}_p - \vec{r}_x|^2}{(\alpha_U r_U)^2}\right) \right)$$

$$U^{\alpha,off} = -U^{\alpha,on}(\vec{r}_p - \vec{r}_x) \tag{2}$$

$$N_U = \frac{\alpha_U^2}{\alpha_U^2 - 1} \tag{3}$$

with $\alpha \in \{\text{left, right}\}$, $\beta \in \{\text{on, off}\}$ and N_U an appropriately choosen normalization constant. The OFF-ganglion cell profiles are just the inverse. These profiles correspond to neurobiological experiments, which showed such receptive field structures (Livingstone and Hubel, 1988). The profiles[1] are normalized to yield a vanishing response to constant illumination, hence they represent contrast filters in the visual pathway. Also separate ganglion cell layers of ON- and OFF-center neurons are implemented, where an OFF receptive field is just the inverse of an ON field. All ON- and OFF-filters are identical and fixed. The afferent postsynaptic potential $h_x(\vec{r}_x)$ ($\vec{r}_x$: location of the cell) of the ganglion cells is then calculated by

$$h_x^{\alpha,\beta}(\vec{r}_x) = x_{\mathrm{sp}} + \sum_{\vec{r}_p} \mathrm{U}^{\alpha,\beta}(\vec{r}_x, \vec{r}_p) p^{\alpha}(\vec{r}_p) = x_{\mathrm{sp}} + x_{\mathrm{aff}}^{\alpha,\beta}(\vec{r}_x), \tag{4}$$

where again $\alpha \in \{\text{left, right}\}$, $\beta \in \{\text{on, off}\}$ and $U^{\alpha,\beta}(\vec{r}_x, \vec{r}_p)$ embodies the DOG profile.

An important determining parameter of the DOG profiles is the so-called total center radius r_{0U},

$$r_{0U} = r_U \sqrt{2 N_U \ln \alpha_U} \tag{5}$$

which defines the border between center and surround region and determines the type of the receptive field structure obtained (Stetter *et al.*, 1993). x_{sp} is a constant parameter[2], which represents an average spontaneous activity of ganglion cells as several investigators demonstrated a relatively high spontaneous activity of these neurons (Kandel *et al.*, 1995).

---

[1] The radius of the inner Gaussian was fixed to 1.8, and the radius of the outer Gaussian to 3.6 yielding a ratio $\alpha_U = 2$ in accord with neurophysiological results. The unit is one grid point.

[2] $x_{\mathrm{sp}} = 2.5$ has been used in all simulations.

The LGN layers

For simplicity a near one-to-one correspondence exists in the model between retinal ganglion and corresponding LGN cells. To allow for an unbalanced ON/OFF-response of LGN cells, however, a parameter q^β

$$q^\beta \begin{cases} = 1 \text{ for } \beta = \text{on} \\ \geq 1 \text{ for } \beta = \text{off} \end{cases} \tag{6}$$

is introduced in (4) to modify the afferent postsynaptic potential at each LGN cell according to

$$h_x^{\alpha,\beta}(\vec{r}_x) = x_{\text{sp}} + q^\beta \cdot x_{\text{aff}}^{\alpha,\beta}(\vec{r}_x). \tag{7}$$

This accounts for the experimental observation by Miller [Miller 1996] that in ferrets OFF-LGN cells fire three to four times more frequent than ON-cells during the time when ON- and OFF-pathways begin to segregate.

Most important, however, interactions between the different LGN cell layers exist in the model. Each LGN neuron possesses vertical interlayer connections between corresponding cells in both layers. These non-modifiable synaptic weights[3] are denoted as g_i with $i \in [1,4]$, where $g_1 = 1.0$ means the self-coupling, $g_2 < 0$ the coupling to the cell of same eye/other type, $g_3 < 0$ to the cell of other eye/same type, and $g_4 < 0$ to the cell of other eye/other type. Therefore the total LGN cell activity is calculated according to

$$x^{\alpha,\beta}(\vec{r}_x) = T_x\left(\sum_{\alpha,\beta} g_{i(\alpha,\beta)}\, h_x^{\alpha,\beta}(\vec{r}_x)\right). \tag{8}$$

The intra-LGN connections between different layers represent inhibitory interactions in accord with neurophysiological results (Pape and Eysel, 1986). Such couplings were already used by Piepenbrock *et al.* (1996a). The function $T_x(\ldots)$ represents a semi-linear activation function, which ensures non-negative LGN cell activities:

$$T_x(x) = \begin{cases} 0 & \text{for } x \leq 0 \\ N_x \cdot x & \text{for } x > 0 \end{cases} \tag{9}$$

The parameter[4] N_x is useful for adjusting the convergence behaviour of the network model. Therefore the model LGN cells are represented by semilinear neurons with positive activities only in accord with neurobiological findings, where a nearly linear response behaviour of LGN cells has been demonstrated (Kandel *et al.*, 1995).

The cortical layer

Finally the efferent conncetions of the LGN-cells converge onto cortical neurons and are plastic. Their non-negative weights, corresponding to exclusively excitatory afferents of the cortical neurons, are denoted as $w^{\alpha,\beta}(\vec{r}_y, \vec{r}_x)$, where again $\alpha \in$ {left, right}, $\beta \in$ {on, off}. $\vec{r}_y$ and $\vec{r}_x$ describe the locations of the cells within the cortex layer and the LGN layers. The modification of these randomly initialized weights is controlled by a learning rule to be specified later. Their spatial structure determines the classic receptive field organization of the cortical neurons into ON/OFF subfields, though these structures would have to be convolved with the DOG profile of the underlying contrast filters to obtain cortical receptive fields (Stetter *et al.*, 1993). However, their essential structure does not change upon this transformation.

The input stimuli lead to an afferent postsynaptic potential h_y^{aff} given by

$$h_y^{aff}(\vec{r}_y, t) = \sum_{\alpha,\beta}\left[\sum_{\vec{r}_y}\left(A(\vec{r}_x - \vec{r}_y)\, w^{\alpha,\beta}(\vec{r}_y, \vec{r}_x, t)\, x^{\alpha,\beta}(\vec{r}_x, t)\right)\right], \tag{10}$$

with t denoting sequential update cycles. The finite size of the afferent arbor may be characterized by a Fermi-function (Stetter *et al.*, 1993) with an arbor radius[5] r_{A0}

$$A(\vec{r}_y, \vec{r}_x) = \begin{cases} \frac{1}{1+\exp((|\vec{r}_x - \vec{r}_y| - r_{A0})/0.3)} & \text{for } |\vec{r}_x - \vec{r}_y| \leq r_{A0} \\ 0 & \text{for } |\vec{r}_x - \vec{r}_y| > r_{A0} \end{cases}. \tag{11}$$

Within the cortex layer there are also plastic lateral interactions. Each neuron thus receives lateral input via both inhibitory and excitatory synaptic connections within a finite radius. The excitatory or inhibitory coupling strength between a postsynaptic cortical neuron at $\vec{r}_y$ and a presynaptic cortical neuron at $\vec{r}_{y'}$ is denoted by $v_E(\vec{r}_y, \vec{r}_{y'})$ or $v_I(\vec{r}_y, \vec{r}_{y'})$, respectively. These weights are all non-negative.

[3] $g_1 = 1$, $g_2 = -0.15$, $g_3 = -0.15$ and $g_4 = -0.15$ have been used in most simulations if not stated otherwise in the text.

[4] $N_x = 0.5$ has been used in most simulations. However, results were robust against any variation of this parameter.

[5] $r_{A0} = 4.0$ has been used in all simulations.

Both excitatory and inhibitory lateral couplings exist within circular regions with radii r_{LE} and r_{LI}. To avoid biasing mexican-hat-like lateral coupling structures by choosing $r_{LE} < r_{LI}$ (Sirosh and Miikkulainen, 1994; Sirosh and Miikkulainen, 1997; Somers *et al.*, 1995) both excitatory as well as inhibitory coupling radii are assumed equal, i.e. $r_{LE} = r_{LI}$ has been set (Burger *et al.*, 1997a; Burger and Lang, 1997b; Burger and Lang, 1999). The excitatory connections are modifiable, while the inhibitory weights form a fixed Gaussian distribution[6] around each cortical neuron. The latter thus represents a global lateral inhibition mediated by cortical interneurons. Furthermore the variable v_{EI} is introduced, representing sort of an effective lateral coupling strength, to allow a more convenient evaluation of the lateral coupling structure:

$$v_{EI}(\vec{r}_y, \vec{r}_{y'}) = v_E(\vec{r}_y, \vec{r}_{y'}) - v_I(\vec{r}_y, \vec{r}_{y'}). \tag{12}$$

Including these lateral connections, the total postsynaptic potential h_y^{tot} of a model cortical cell is, for computational reasons, approximated by

$$\begin{aligned} h_y^{tot}(\vec{r}_y, t) &= h_y^{aff}(\vec{r}_y, t) + \sum_{\vec{r}_{y'} \neq \vec{r}_y} \left(v_{EI}(\vec{r}_y, \vec{r}_{y'}, t)\, h_y^{aff}(\vec{r}_{y'}, t) \right) \\ &= h_y^{aff}(\vec{r}_y, t) + h_y^{lat}(\vec{r}_y, t) \end{aligned} \tag{13}$$

with $h_y^{aff}(\vec{r}_y, t)$ the postsynaptic potential due only to afferent inputs at cortical position $\vec{r}_y$ and $h_y^{lat}(\vec{r}_y, t)$ the corresponding postsynaptic potential at update step t mediated via lateral couplings to nearby neurons. The diskrete time variable $t = 0, 1, 2, \ldots$ in (10) and (13) denotes sequential update cycles. The corresponding cell activity is then given by

$$y(\vec{r}_y, t) = T_y\left(h_y^{tot}(\vec{r}_y, t) \right) \tag{14}$$

with the function $T_y(\ldots)$ representing a piecewise linear approximation to a sigmoidal activation function:

$$T_y(h_y^{tot}) = \begin{cases} 0 & \text{for } h_y^{tot} \leq \theta_1 \\ h_y^{tot} - \theta_1)/(\theta_2 - \theta_1) & \text{for } \theta_1 < h_y^{tot} < \theta_2 \\ 1 & \text{for } h_y^{tot} \geq \theta_2 \end{cases}. \tag{15}$$

This function introduces an essential nonlinearity into the response of a cortical neuron. The lower threshold θ_1 is chosen to be modifiable[7] in order to take into consideration that neurons can become accustom to a continual high input activity. θ_1 increases, if there is a high input activity, and it decreases, if there is a low input activity, according to a learning rule, which will be specified later. In this way sort of a conscience mechanism (DeSieno, 1988) is implemented in a simple manner.

Note that only the total postsynaptic potential is transformed via the non-linear activation function to result in the activity of the cortical neuron considered. This approximation to the true postsynaptic potential is chosen for computational convenience. The correct postsynaptic potential would have to be calculated with the activities $y(\vec{r}_{y'}, t)$ of neighboring cortical neurons instead of their postsynaptic potentials $h_y^{aff}(\vec{r}_{y'}, t)$. As will be shown later, the activities of model cortical neurons always stay close to the lower activation threshold, hence operate in the linear range of the activation function. In this activity regime postsynaptic potential and activity are equivalent, then. The mathematical convenience gained is a simple, easy to evaluate expression – in parallel mode – for the activity of the model cortical neurons instead of an implicit equation. The latter would have to be iterated several times for the activity to settle into a steady state. Each output activity would then have to be evaluated sequentially, which would introduce strong dependences on the order of evaluation, hence complicating further a consistent evaluation of the activities of all output nodes. The postsynaptic potential so calculated thus represents an upper bound to the true potential. The latter would result in even sharper activity blobs as discussed later on. Further note that afferent $h_y^{aff}(\vec{r}_y, t)$ and lateral $h_y^{lat}(\vec{r}_y, t)$ postsynaptic potentials are evaluated at equal times to become combined to the total postsynaptic potential. This is justified as long as any signal delays from neighboring neurons are short compared to the update cycle of the discretized simulation dynamics. This approximation is intended to simulate

[6] The lateral coupling existed within a radius of 12.0 grid points. The coupling sums were $C_E = C_I = 12.0$ for each connection type. The radius of the inhibitory lateral couplings forming a spatial Gaussian distribution was 8.0, and the plastic excitatory lateral couplings were initialized as a spatial Gaussian distribution with radius 3.0.

[7] The initial value is $\theta_1 = 0$.

in the model recent investigations which showed that a cortical response to a visual stimulus appears faster than delayed intracortical signals can influence it (Oram and Perrett, 1994). As a technical aside, given random uncorrelated input stimuli, only then pronounced activity blobs, forming in the ganglion/LGN model layer due to overlapping center-surround input filters, could be observed in the cortical model layers, too. Note, that in the linear version ($y(\vec{r}_y, t) = h_y^{tot}(\vec{r}_y, t)$ of the model (Burger and Lang, 1999) the intracortical connections mediated lateral inputs corresponding to cortical activity values of the update cycle before in order to take runtime delays of lateral signals into account. In this case activity blobs did not appear as any two random input stimuli presented sequentially are uncorrelated, hence destroy, in the cortical model layers, any correlations existing within the ganglion/LGN model layers. It will be argued later, that these activity blobs form an essential ingredient to obtain spatially oscillating intracortical coupling structures and realistic orientation map structures in the nonlinear version of the model with adaptable lateral couplings.

The learning rules

Each update cycle starts with the presentation of uncorrelated, non-negative, equally distributed, random activities within the interval [0.0, 1.0] to the input layer. Then, after the calculation of the activity values of each cell, the afferent synaptic weights of the cortical neurons are updated according to a learning rule described below.

The afferent synaptic weights

To obtain an update rule for the afferent weights we expand the corresponding constant sum (CS) rule (16), which has been used earlier for the modification of the lateral weights (Burger and Lang, 1999), in powers of η and neglect all terms of order $O(\eta^2)$ and higher:

$$w_i(t+1) = C_w \cdot \frac{w_i(t) + \eta y(t) x_i(t)}{\Sigma_j [w_j(t) + \eta y(t) x_j(t)]}, \tag{16}$$

yielding

$$w_i(t+1) = C_w \cdot \frac{w_i(t)}{\Sigma_j w_j(t)} + \eta C_w y(t) \left[\frac{x_i(t)}{\Sigma_j w_j(t)} - \frac{1}{\{\Sigma_j w_j(t)\}^2} w_i(t) \sum_j xj(t) \right] \tag{17}$$

with C_w in (16) representing the constant coupling sum[8]

$$C_w := \sum_j w_j(t=0) = \sum_j w_j(t). \tag{18}$$

Strictly speaking (18) is not exactly kept constant if rule (17) is used. With a small enough learning rate parameter[9] η, however, (18) is valid to good approximation. This finally yields the following update rule for the afferent weights:

$$\begin{aligned} w_i(t+1) &= w_i(t) + \eta y(t) \left[x_i(t) - \frac{1}{C_w} w_i(t) \sum_j x_j(t) \right] \\ &= w_i(t) + \eta y(t) [x_i(t) - \lambda w_i(t)] \end{aligned} \tag{19}$$

with $\lambda = \Sigma_j x_j(t) / \Sigma_j w_j(t)$ representing, after convergence, the largest eigenvalue of the correlation matrix of the input activities. In (16), (17) and (18) Σ_j represents the sum over the whole afferent tree of the cortical neuron considered.

Note that the expansion is essential to obtain a local learning rule which does not depend on the afferent coupling strenghts of all other cortical neurons as is the case with (16).

Also note, that the decay term of this Hebbian learning rule includes the sum over all LGN cell activities $\Sigma_j x_j(t)$. Without any spontaneous activity $x_{sp} = 0$ and OFF cell strengthening in (4) and without any transfer function $T_x(\ldots)$ in (8), this sum would be zero because of the exact balance of the ON- and OFF-fields:

$$x_j^{on}(t) = -x_j^{off}(t) \Rightarrow \sum_j x_j(t) = 0. \tag{20}$$

This would lead to an unconstrained Hebbian learning then. Thus in a model with purely linear LGN neurons the afferent weights to cortical model neurons cannot be trained by rule (19).

[8] The afferent coupling sum has been fixed to $C_w = 0.1$.
[9] The learning rate parameter has been fixed to $\eta = 0.001$ in all simulations.

The activation thresholds

The lower threshold θ_1 of the activation function (15) is modified according to

$$\theta_1(\vec{r}_y, t+1) = \theta_1(\vec{r}_y, t) + \eta_{\theta_1} \cdot y(\vec{r}_y, t+1) - D_{\theta_1}, \quad (21)$$

where $\eta_{\theta 1}$ is a learning rate and $D_{\theta 1}$ a subtractive constraint. The latter leads to a decrease of θ_1, if the cell is barely active. But a cortical neuron becomes more insensitive to input stimuli, hence its activation threshold increases, if it was well stimulated in the past. The upper threshold has been fixed to $\theta_2 = 1.0$ in most simulations as cortical activities turned out to never saturate, thus an initially modifiable threshold showed no decernable effect concerning the results.

The intracortical synaptic weights

The excitatory lateral couplings of the cortical cells are update with a stabilized Hebbian learning rule with constant sum constraints (CS) in close analogy to (16):

$$(\vec{r}_y, \vec{r}_{y'}, t+1) = C_E \cdot \frac{v_E(\vec{r}_y, \vec{r}_{y'}, t) + \eta_{\text{lat}} y(\vec{r}_y, t) y(\vec{r}_{y'}, t)}{\sum_{\substack{\vec{r}_{y'} \\ |\vec{r}_{y'} - \vec{r}_y| \le r_{LE}}} [v_E(\vec{r}_y, \vec{r}_{y'}, t) + \eta_{\text{lat}} y(\vec{r}_y, t) y(\vec{r}_{y'}, t)]} \cdot (22)$$

η_{lat} denotes the learning rate parameter which has been fixed to $\eta_{\text{lat}} = 0.1$. The factor C_E denotes the sum of excitatory intracortical synaptic coupling strengths of any cortical neuron:

$$C_E = \sum_{\substack{\vec{r}_{y'} \\ |\vec{r}_{y'} - \vec{r}_y| \le r_{LE}}} (v_E(\vec{r}_y, \vec{r}_{y'})). \quad (23)$$

This sum was independently kept constant[10] at every cortical cell during the whole simulation. It introduces a competition between the synaptic weights for the total amount of available coupling strengths.

This learning rule corresponds to the one used earlier (Burger *et al.*, 1997a; Burger and Lang, 1997b; Burger and Lang, 1999). Also Sirosh and Miikkulainen (1994), (1997) implemented this rule in their LISSOM model. In recent investigations we also tested a Yuille-like stabilized Hebbian rule (Burger *et al.*, 1997a) for the modification of the lateral weights without such a strong contraint as used by the CS rule. But in this case it was very difficult to get a stable numerical convergence of the synaptic weight vectors, because of a strong competition between the afferent and the lateral weights.

[10] The sum of excitatory lateral coupling strengths has been fixed to $C_E = 10$.

Results

All layers of the network model considered comprised 32 × 32 neurons. In order to avoid boundary artifacts periodic boundary conditions were imposed. Also, each simulation comprised 20000 iterations and convergence was controlled by monitoring the normalized magnitude of consecutive weight vector changes averaged over all cortical neurons. After 2000 iterations already receptive field structers were mature but cortical feature maps developed only afterwards though without further changes in the normalized magnitude of weight vector changes.

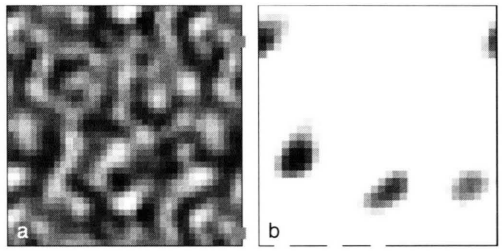

Fig. 2. Examples for the activity structure of a ganglion/LGN layer (a) and of the cortex layer (b). The intensity of color denotes the strength of the activity values, where white means no activity.

After presenting random stimulus patterns to the input layer of the network, ganglion/LGN cells, functioning as contrast filters, processed these stimuli by removing any finite average activity corresponding to a constant illumination within the visual field. Their output activities are thus characterized by fluctuations in brightness within the stimulus pattern plus some positive spontaneous activity. As the receptive fields of these contrast filters overlap strongly, correlated output activities result. Therefore a pronounced activity structure formed yielding a system of stripes of high activity against a background of low activity (Fig. 2). Nearly all neurons were activated in some way, however. This corresponds with neurophysiological findings, which reported a high spontaneous activity of ganglion cells (Kandel *et al.*, 1995).

Receptive field formation

In a first set of simulations no interaction ($g_{i(\alpha,\beta)} = 0$) between LGN cells and no strengthening ($q^{off} = 1$) of the activities of OFF-LGN cells were considered. The LGN cell efferents converged on cortical neurons within an arbor radius of 4.0 grid points. The piecewise linear activation function of the cortical simple cells with a finite activation threshold ensured non-negative activity values and prevented the firing of neurons in response to only weak afferent activites. In contrast, blobs of pronounced activities emerged whenever strong input activity appeared (Fig. 2) as have been observed in neurobiological investigations, too (Grinvald *et al.*, 1988). Note that most former network models, refered to in the introduction, did not describe such activity structures.

The activities of model cortical simple cells did not exceed the lower threshold θ_1 of the activation function much in most cases lending support to the afore mentioned approximation to the total postsynaptic potential of any model cortical neuron. Thus cortical activities did not saturate during the course of the simulations in accord with results of neurobiological experiments. Therefore the formal upper threshold θ_2 turned out to play a minor role only. Consequently, θ_2 was not modified during a simulation run.

The effect of inhibitory LGN interactions and an ON/OFF imbalance

The receptive field profiles of model cortical simple cells were segregated into two or three lobes mostly. But without couplings between LGN neurons or strengthened OFF-LGN-cells a great majority of the afferent connections are dominated by ON-LGN-cells. As a result these model cortical simple cells were only weakly orientation selective. With inhibitory connections between LGN cells of same eye and other type adjusted to $g_2 = -0.45$ a better segregation could be reached.

Instead of LGN inhibition a general strengthening of the OFF-pathway could also support the segregation of cortical receptive fields. Already a strengthening of the OFF-afferents by two percent relative to ON-afferents (i.e. $q = 1.02$) was sufficient to yield bi- and trilobed receptive field profiles without a dominance of one type of afferents. If OFF-afferents were strengthened in addition to setting $g_2 \geq -0.45$, then q^{off} had to be as large as $q^{off} = 1.20$ in order for the latter to become effective. Thus the receptive field segregation was basically driven by the intra-LGN inibition and only fine tuned by the OFF cell strengthening.

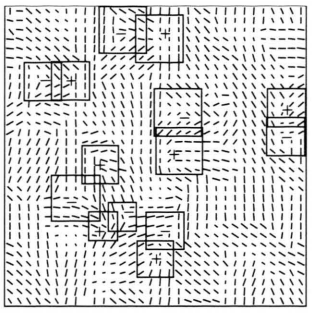

Fig. 3. Simulated orientation map. The direction of the lines denotes the orientation preference of the corresponding cortical neuron. The preferences were determined by using sine waves as input stimuli. Thus the lines respresent preferred orientations perpendicular to the wave front, which caused the maximal response. The length of the lines denotes the orientation selectivity of the cells, calculated as the ratio of maximal and minimal response. Furthermore some vortex structures are marked.

The Formation of orientation maps

The effect of adaptive intracortical couplings

This segregation of ON/OFF-afferents into spatially oscillating receptive field structures led to orientation-selective cortical neurons then. Without any intracortical interaction $v_{EI}(\vec{r}_y, \vec{r}'_y) = 0$, however, no self-organization of these orientation preferences into continuous orientation maps within the cortex layer resulted. But using adaptive lateral connections the orientation preferences became organized and a realistic orientation map developed (Fig. 3). The map contained isoorientation domains and linear zones as well as pinwheel vortices, saddle points and fracture lines. Note, that ± 1/2 vortices occured exclusively, mostly in pairs of opposing sign again corroborating experimental findings (Obermayer and Blasdel, 1997). Though the simulated patch of cortex is certainly too small, a Fourier transformation of the orientation preference structure showed signs of an existing periodicity in the orientation map.

The orientation preferences[11] and of single cortical cells were affected by the intracortical couplings. Determining the preferences with regard to afferent coupling strengths only, hence without any consideration of lateral conncetions, led to orientation preferences different from those obtained including lateral couplings. Thus the classic cortical receptive field is not necessarily the decisive factor of a cell's orientation preference.

The lateral interaction also influenced the development of receptive field profiles. The field structures obtained represent bi- and trilobed profiles mostly and neighboring fields showed a clear overlap maximization leading to a pronounced phase locking (Fig. 4).

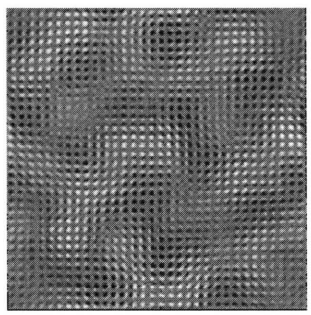

Fig. 4. Receptive field structures of the cortical neurons. The intensity of grey values denotes the strength and the type of the afferent couplings. A mean grey value signifies no connection, a lower intensity a dominance of OFF cell connections, and a higher intensity a dominance of ON cell connections. A clear segregation of ON/OFF subfields and a remarkable phase locking can be seen. See text for details.

This feature enabled a cortical neuron to represent more than one spatial frequency inspite of an identical arbor radius for all cortical neurons. Thus preferred spatial frequencies spanning a range of 0.7 octaves, roughly, resulted. Compared to a range of roughly 3 octaves (von der Heydt *et al.*, 1992) of experimentally observed preferred spatial frequencies these smaller values resulted from a too small arbor radius choosen. Using a larger radius, requiring larger simulated cortical patches, though, would leave more space for a wider frequency range to be represented. However, we did not try to improve on this aspect of the simulation results further because of excessive memory and CPU time requirements. Each spatial frequency tuning curve in addition was characterized by a half width at half maximum (HWHM) of 1.0–1.5 octaves (Fig. 5) corresponding well to experimentally observed tuning widths (Field and Tolhurst, 1986; De Valois *et al.*, 1982; Daugman, 1985).

Another effect of an adaptable lateral interaction was a drastic narrowing of the orientation tuning curves (Fig. 6). Without any intracortical synaptic connections a rather broad tuning curve with an average HWHM = 50°–60° occured (Fig. 6d). Such broad tuning curves typically result also with fixed mexican-hat-like intracortical interactions. In the current network model, instead, a relatively broad distribution of tuning curves with HWHM values peaking around 40° resulted. Thus many cells existed with HWHM = 15°–55°. This broad distribution with many sharply tuned neurons did not result from simulations with no lateral interactions. Swindale recently reported orientation tuning curves with HWHM values of 10°–50° observed in cats (Swindale, 1998). Hence our results are well in accord with these neurobiological results. Note, that in case of incongruent monocular orientation maps, as they result from vanishing intra-LGN couplings, more than one peak in a tuning curve may result, because both monocular orientation preferences of one cortical cell resulting from left and right eye afferents could differ (Fig. 6a, b). Some minor secondary peaks (see peak at 165° in (6c)) observed occasionally in case of congruent monocular maps could be shown to result from a limited size of characteristic map structures like iso-orientation domains, linear zones etc. compared to the range of lateral cortical interactions as has been verified by varying the latter in different simulations.

The effect of inhibitory LGN couplings

Earlier versions of the network model produced ongoing strong fluctuations resulting in a permanent reorganization of the orientation map. While the qualitative structure of the map remained, the detailed structure like the position of vortices, for example, was constantly changing. With the current network model, however, such strong structural fluctations were never observed. Even with relatively strong intra-LGN connections (e.g.

[11] They have been obtained by determining response amplitudes of cortical neurons to sinusoids presented with orientations varied in steps of 4 deg.

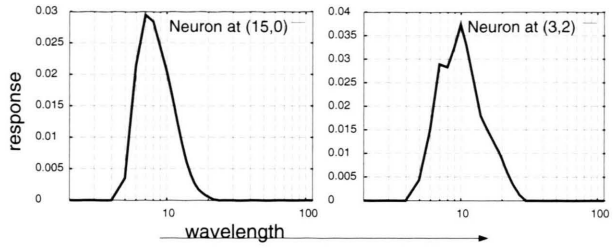

Fig. 5. Spatial frequency tuning curves of two neurons contained in Fig. 4 or Fig. 3, respectively. The neural response values were calculated by presenting sine waves oriented in the direction of the orientation preference as input stimuli. The wavelength of the waves is given in units of grid points. The location of the cells in the orientation map is denoted by coordinates (row, column), beginning at the upper left corner with (0,0).

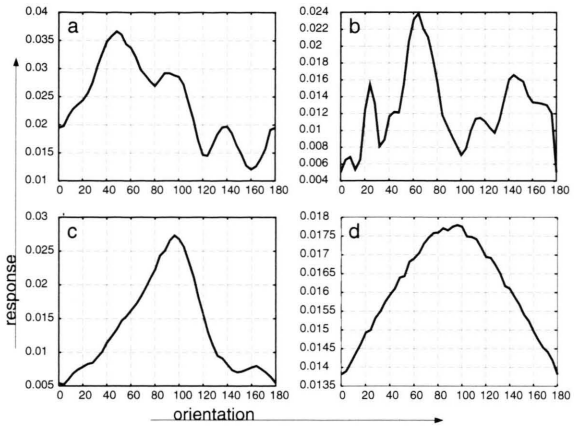

Fig. 6. Orientation tuning curves of several cortical neurons. The neural response values were calculated by presenting sine waves with the preferred stimulating wavelength as input stimuli. (a), (b) Two examples of tuning curves simulated without any intra-LGN couplings but with a strengthening of the OFF cells resulting in incongruent monocular orientation maps. (c) A typical tuning curve simulated with intra-LGN connections and strengthened OFF cells resulting in congruent monocular orientation maps. (d) The same situation as in (c), but calculated only with afferent inputs.

$g_2 = -0.45$) only weak fluctuations ocurred. Furthermore without intra-LGN couplings both monocular orientation maps always were decorrelated, meaning that many cortical neurons experienced two distinct monocular orientation preferences. In the current network model this could be prevented by introducing intra-LGN couplings between LGN cells of other eye and type (i.e. g_4). Inhibitory couplings between LGN cells of different eyes were described by Pape and Eysel (1986), hence are motivated neurobiologically. Already a weak interaction ($g_4 = -0.05$) led to congruent monocular orientation preference maps corresponding to experimental results of Gödecke and Bonhoeffer (1996). In contrast, Soodak (1987) reported non-conforming monocular maps. Also Pettigrew (1974) reported monocular receptive fields of newborn kittens which were misaligned by as much as 30°.

Concerning the distribution of orientation preferences represented by model cortical neurons forming the orientation map a slight over-representation of some preferred orientations were mostly observed in the simulations described above. This is certainly due to the limited size of the simulated patches of cortex resulting in an insufficient averaging of all orientations represented.

Ocular dominance patches

Although many cortical neurons showed some eye preference in the simulations, anatomic ocular dominance did not develop to any substantial degree. Only a physiological eye preference could be obtained. The ocular dominance index (ODI) histograms peaked around zero but showed finite values up to 0.7 (Fig. 7).

In case of conforming monocular orientation maps more binocular cortical cells emerged than in other cases. Furthermore cells possessing the same eye preference formed stripe-like patchy clusters. Again a Fourier transformation of the ocular dominance structure pointed to the existence of a decent periodicity. The simultaneous development of both ocular dominance and orientation preference seemed to be decoupled, though, since vortices of orientation maps were localized within ocular dominance clusters as well as at their boundaries (Fig. 8).

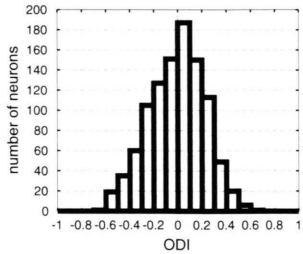

Fig. 7. Ocular dominance index histogram. −1 denotes pure left monocular cells, 1 pure right monocular cells, and 0 exact binocular cells. See text for details.

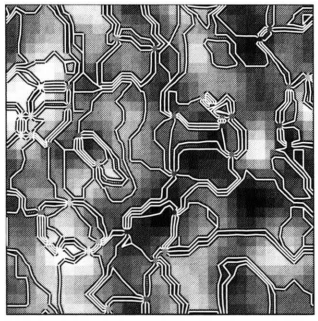

Fig. 8. Ocular dominance structure with overlain iso-orientation map corresponding to the map in Fig. 3. The grey intensity denotes the ODI value, where white signifies ODI = −1 and black ODI = +1.

In linear CBL network models vortex structures are always localized preferentially at the boundaries of ocular dominance clusters (Stetter *et al.*, 1994; Stetter *et al.*, 1995; Burger and Lang, 1999). Though the current results do not show such strong correlations either result still disagrees with results of optical imaging studies of feature maps in adult mammals, which show vortices in the center of ocular dominance bands (Obermayer and Blasdel, 1993; Erwin *et al.*, 1995). Only SOM-like models, normalizing across all features, yield vortices preferentially in the center of ocular dominance bands. However, note that the simulations presented in this study correspond to a prenatal developmental situation. Therefore the extent as well as the vortex localization need not necessarily correspond to postnatal mature cortical feature maps. Finally, also with Piepenbrock's ocular dominance parameter set relating to the g_i variables ($g_i = -0.15$, $\forall i \neq 1$) no stronger ocular dominance resulted.

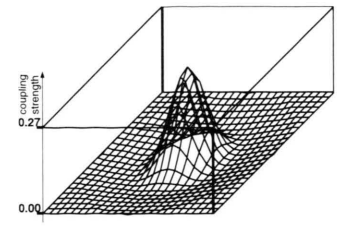

Fig. 9. Lateral coupling structure. The lateral coupling structures of all cortical neurons developed to nearly perfekt DOG profiles. Positive values denote an excitatory connection, negative values an inhibitory.

Local cortical circuits

Initializing the excitatory lateral synaptic weights, two starting configurations were considered. Either excitatory weights were initially confined to a narrow Gaussian distribution centered around any cortical neuron considered or all excitatory weights had about equal strengths up to the maximal radius of the interaction. The former situation was intended to simulate a spreading out of growing excitatory connections within the maximal range of the interaction. The inhibitory weights were always initialized as a broad Gaussian distribution extending to the maximal radius of both lateral interactions. In every case spatially oscillating DOG-like lateral coupling profiles emerged (Fig. 9). The basic driving force for the formation of a Gaussian coupling profile of excitatory coupling strengths was the existence of locally confined cortical activity blobs, which led to a strengthening of lateral weights to nearby neurons within the blob. Note that a nonlinear cortical activation function is an essential ingredient to obtain these localized activity structures, as they cut off any low, sub-threshold level activities. If this activation threshold is lowered, large shallow activity blobs as well as too many blobs within the cortex layer appeared and led to a deformation of the resulting DOG profile. Finally, the DOG structure of lateral coupling profiles led to the orientation map organization described above.

Discussion and Conclusion

In this study we presented a non-linear incremental Hebbian learning neural network model with the simultaneous and activity-dependent development of modifiable afferent and intracortical syn-

aptic connections into orientation-selective receptive field structures and cortical feature maps. The model incorporates essential neurobiological findings and leads to realistic orientation maps and cortical activity blob structures which develop simultaneously with the emergence of local intracortical synaptic coupling circuits. Thus the model allows the simulation of the simultaneous development of many features which have been described only separately in several recent network models since.

In the current model the organization of cortical orientation-selectivity is driven by spontaneous uncorrelated activities of retinal cells. As discussed in the introduction already, retinal ganglion cell activity waves recently described are probably too large in their extent to drive the development of orientation-selective cortical simple cells (Miller, 1994). The activity-dependence of ocular dominance patches is well founded, but its role during the formation of orientation preference and selectivity maps is still in disput (Weliky and Katz, 1997; Crair *et al.*, 1998). Indications in favour of such an activity-dependence were found by several investigators (Braitenberg and Schütz, 1991; Chapman and Stryker, 1993). Also Miller advocated these ideas (Miller, 1992; Miller, 1995). He described the orientation-selectivity as resulting from a competition of ON- and OFF-cells. In case of cats the competitive inputs come from the LGN, in case of monkeys from cortical layers without orientation selectivity. But he thought that the activity-dependence of the basic initialization was still unclear (Miller, 1995). For example, elliptic receptive fields of LGN cells could be seeds of orientation selectivity. Our model does not need any structured initialization but generates the receptive field profiles out of randomly initialized synaptic weights as first shown by Linsker (Linsker, 1986). Models using structured or oriented input stimuli respectively (Somers *et al.*, 1995; Sirosh and Miikkulainen, 1994; Sirosh and Miikkulainen, 1997) get into difficulties, if they should explain the emergence of orientation selectivity in the absence of structured visual stimuli.

The orientation tuning curves of many model cortical neurons exhibited HWHM = 20° – 45° well in accord with experimentally observed tuning widths. In addition the spatial frequency tuning of model cortical neurons exhibited realistically small tuning curves with a HWHM range of about one octave also in close correspondence to neurophysiological results. The phase locking of neighboring cortical receptive fields due to the overlap maximization mechanism led to deformed bi- or trilobed receptive fields and enabled the coding of various spatial frequencies without a concomittant variation of corresponding arbor radii. The range of preferred spatial frequencies encoded by model cortical neurons in the simulations was not always sufficiently broad to conform to experimental values. This deficiency could be remedied, however, by using larger receptive field sizes. This issue could not be persued further because of prohibitively long simulation runs necessary for model layers larger than 64×64 neurons in each layer.

Depending on the parameters chosen aligned as well as misaligned monocular orientation maps could be obtained in the simulations. The primary parameter proofed to be the inhibition between LGN cells of different type and eye. Concerning the experimental situation it seems still unclear, wether both monocular orientation maps conform to each other in the prenatal visual cortex (Gödecke and Bonhoeffer, 1996, Pettigrew 1974; Pape and Eysel, 1986). The presented neural network model can simulate both situations, and thus we offer a proposition for the role of intra-LGN inhibition on this matter.

The model also succeeded in simulating the emergence of realistic spatially oscillating intracortical coupling circuits. Until now, only Sirosh and Miikkulainen (1994), (1997) described the development of lateral coupling structures well represented by a DOG. But their competitive LISSOM model needed structured input stimuli and did not explain the development of orientation-selective receptive fields. Especially there were no segregated ON- and OFF-LGN layers. The simultaneous emergence and development of orientation-selectivity and self-organization of lateral DOG circuits has not been described in the literature so far. Localized activity blobs forming even in response to random, uncorrelated input activities are an essential ingredient driving the formation of DOG profiles in lateral coupling structures. These DOG profiles are essential to supervise the grouping of the orientation selectivity into realistic orientation maps.

However, ocular dominance was only weakly represented in the simulated feature maps. This

situation is similar to the visual cortex of cats, where investigations (Hubel, 1982; Livingstone and Hubel, 1988) did not yield a strong eye preference of most cortical simple cells as it has been found in case of monkeys. Note, however, that the cortical input layer IVc of the striate cortex of monkeys contains many monocular simple cells which do not possess a strong orientation specificity. In other cortical layers with highly orientation-selective neurons the amount of neurons with a strong ocular dominance is less pronounced (Hubel, 1982; Livingstone and Hubel, 1988). Thus the lack of any strong anatomically defined ocular dominance in our model cortical layer is not necessarilly in disagreement with neurobiological results. Apart from this, the simulated map of physiological ocular dominance contains stripe-like patches possessing a periodic order. Similar ocular dominance patches were found in the visual cortex of the cat, too (LeVay *et al.*, 1978).

In summary some characteristic features of cortical simple cells, concomittant cortical feature maps and local cortical circuitry were simulated within a biologically inspired neural network model. Driven by random stimulus patterns only, realistic cortical feature maps as well as spatially oscillating intracortical coupling structures self-organized simultaneously in an activity-dependent manner. Care has been given to account for as many experimental findings as possible. Some of these features were included in earlier network models only occasionally, mostly affording specific assumptions and/or a special architecture. Though the subject has been treated in much detail in the literature, no single model network has since been described which delt with all these features simultaneously.

Blasdel G. G. (1992), Differential imaging of ocular dominance and orientation selectivity in monkey striate cortex. J. Neurosci. **12**, 3115–3138.

Bonhoeffer T. and Grinvald A. (1991), Iso-orientation domains in cat visual cortex are arranged in pinwheel-like patterns. Nature **353**, 429–431.

Braitenberg V. and Schütz A. (1991), Anatomy of the Cortex: Statistics and Geometry. Springer, New York, Berlin, Heidelberg.

Burger T. (1999), Selbstorganisation von Orientierungskarten und Gratingzellen im visuellen Kortex: Nichtlineare neuronale Netzwerkmodelle mit adaptiven afferenten und lateralen Kopplungen. Logos Verlag, Berlin.

Burger T., Kussinger M., Ziegaus C. and Lang E. W. (1997a), Emergence of orientation maps in area 17 of the cerebral cortex: A correlation-based model with afferent and lateral plasticity of synaptical weights and real input patterns. In: Proceedings of the 25th Göttingen Neurobiology Conference (Elsner N. and Wässle H., eds) vol. **2**. Georg Thieme, Stuttgart, New York, p. 1015.

Burger T. and Lang E. W. (1997b), A CBL network model with intracortical plasticity and natural image stimuli. Lecture Notes in Computer Science **1327**, 225–230.

Burger T. and Lang E. W. (1999), An incremental Hebbian learning model of the primary visual cortex with lateral plasticity and real input patterns. Z Naturforsch. C **54**, 128–140.

Callaway E. M. and Katz L. C. (1990), Emergence and refinement of clustered horizontal connections in cat striate cortex. J. Neurosci. **10**, 1134–1153.

Chapman B. and Stryker M. P. (1993), Development of orientation selectivity in ferret visual cortex and effects of deprivation. J. Neurosci. **13**, 5251–5262.

Crair M. C., Deda C. G. and Stryker M. P. (1998), The role of visual experience in the development of columns in cat visual cortex. Science **279**, 566–570.

Daugman J. G. (1985), Uncertainty relation for resolution in space, spatial frequency and orientation optimized by two-dimensional visual cortical filters. J. Opt. Soc. A 2(7), 1160–1169.

DeSieno D. (1988), Adding a Conscience to Competitive Learning. IEEE International Conference on Neural Networks (San Diego 1988). New York: IEEE. vol. I, 117–124.

DeValois R. L., Albrecht D. G. and Thorell L. G. (1982), Spatial frequency selectivity of cells in Macaque visual cortex. Vision Res. **22**, 531–544.

Erwin E., Obermayer K. and Schulten K. (1995), Models of orientation and ocular dominance columns in the visual cortex: a critical comparison. Neural. Comput. **7**, 425–468.

Field D. J. and Tolhurst D. J. (1986), The structure and symmetry of simple-cell receptive-field profiles in the cat's visual cortex. Proc. R. Soc. Lond. B **228**, 379–400.

Fisken R. A., Garey L. J. and Powell T. P. S. (1973), Patterns of degeneration after intrinsic lesions of the visual cortex (area 17) of the monkey. Brain Res. **53**, 208–213.

Gilbert C. D., Hirsch J. A. and Wiesel T. N. (1990), Lateral interactions in visual cortex. Cold Spring Harbor Symposia on Quantitative Biology **55**, 663–677.

Gilbert C. D. and Wiesel T. N. (1989), Columnar specificity of intrinsic horizontal and corticocortical connections in cat visual cortex. J. Neurosci. **9**, 2432–2442.

Gödecke I. and Bonhoeffer T. (1996), Development of identical orientation maps for two eyes without common visual experience. Nature **379**, 251–254.

Grinvald A., Frostig R. D., Lieke E. and Hildesheim R. (1988), Optical imaging of neuronal activity. Physiol. Rev. **68**, 1285–1366.

Hubel D. H. and Wiesel T. N. (1977), Functional architecture of macaque monkey visual cortex. Proc. R. Soc. Lond. B **198**, 1–59.

Hubel D. H. (1982), Exploration of the primary visual cortex, 1955–1978. Nature **299**, 515–524.

Jones J. P. and Palmer L. A. (1987), The two-dimensional spatial structure of simple receptive fields in cat striate cortex. J. Neurophysiol. **58**, 1187–1211.

Kandel E. R., Schwartz J. H. and Jessell T. M. (eds) (1995), Essentials of neural science and behavior. Appleton & Lange, Norwalk.

Katz L. C. and Callaway E. M. (1992), Development of local circuits in mammalian visual cortex. Ann. Rev. Neurosci. **15**, 31–56.

Katz L. C., Gilbert C. D. and Wiesel T. N. (1989), Local circuits and ocular dominance columns in monkey striate cortex. J. Neurosci. **9**, 1389–1399.

LeVay S., Hubel D. H. and Wiesel T. N. (1975), The pattern of ocular dominance columns in macaque visual cortex revealed by a reduced silver stain. J. Comp. Neurol. **159**, 559–576.

LeVay S., Stryker M. P. and Shatz C. J. (1978), Ocular dominance columns and their development in layer IV of the cat's visual cortex. J. Comp. Neurol. **179**, 223–244.

Linsker, R. (1986), From basic networks principles to neural architecture (series). Proc. Natl. Sci. USA **83**, 7508–7512, 8390–8394, 8779–8783.

Livingstone M. and Hubel D. (1988), Segregation of form, color, movement, and depth: anatomy, physiology, and perception. Science **240**, 740–749.

Lund J. S., Yoshioka T. and Levitt J. B. (1994), Substrates for interlaminar connections in area V1 of macaque monkey cerebral cortex. Cerebral Cortex **10**, 37–60.

Malsburg C. von der (1973), Self-organization of orientation sensitivity cells in the striate cortex. Kybernetik **14**, 85–100.

Meister M., Wong R. O. L., Baylor D. A. and Shatz C. J. (1991), Synchronous bursts of action potentials in ganglion cells of the developing mammalian retina. Science **252**, 939–943.

Miller K. D., Keller J. B. and Stryker M. P. (1989), Ocular dominance column development: analysis and simulation. Science **245**, 605–615.

Miller, K. D. (1992), Development of orientation columns via competition between on- and off-center inputs. Neuroreport **3**, 73–76.

Miller K. D. (1994), A model for the development of simple cell receptive fields and the ordered arrangement of orientation columns through activity-dependent competition between on- and off-center inputs. J. Neurosci. **14**, 409–441.

Miller K. D. (1995), Receptive fields and maps in the visual cortex: models of ocular dominance and orientation columns. In: Models of Neural Networks (Domany E., van Hemmen J. L., Schulten K., eds) vol. 3. Springer, New York, Berlin, Heidelberg, pp. 55–78.

Miller K. D. (1996), Synaptic economics: competition and cooperation in synaptic plasticity. Neuron. **17**, 367–370.

Obermayer K. and Blasdel G. G. (1993), Geometry of orientation and ocular dominance columns in monkey striate cortex. J. Neurosci. **13**, 4114–4129.

Obermayer K. and Blasdel G. G. (1997), Singularities in primate orientation maps. Neural. Comput. **9**, 555–575.

Oram M. W. and Perrett D. I. (1994), Modelling visual recognition from neurobiological constraints. Neural. Networks **7**, 945–972.

Pape, H. C. and Eysel U. T. (1986), Binocular interactions in the lateral geniculate nucleus of the cat: gabaergic inhibition reduced by dominant afferent activity. Exp. Brain Res. **61**, 265–271.

Pettigrew J. D. (1974), The effect of visual experience on the development of stimulus specificity by kitten cortical neurons. J. Physiol. **237**, 49–74.

Piepenbrock C., Ritter H. and Obermayer K. (1996a), Cortical map development driven by spontaneous retinal activity waves. Lecture Notes in Computer Science **1112**, 427–432.

Piepenbrock C., Ritter H. and Obermayer K. (1996b), Linear correlation-based learning models require a two-stage process for the development of orientation and ocular dominance. Neural. Proc. Letters **3**, 1–7.

Sirosh J. and Miikkulainen R. (1994), Cooperative self-organization of afferent and lateral connections in cortical maps. Biol. Cybern. **71**, 65–78.

Sirosh J. and Miikkulainen R. (1997), Topographic receptive fields and patterned lateral interaction in a self-organizing model of the primary visual cortex. Neural. Comput. **9**, 577–594.

Somers D. C., Nelson S. B. and Sur M. (1995), An emergent model of orientation selectivity in cat visual cortical simple cells. J. Neurosci. **15**, 5448–5465.

Soodak R. E. (1987), The retinal ganglion cell mosaic defines orientation columns in striate cortex. Proc. Natl. Acad. Sci. USA **84**, 3936–3040.

Stetter M., Lang E. W. and Müller A. (1993), Emergence of orientation selective simple cells simulated in deterministic and stochastic neural networks. Biol. Cybern. **68**, 465–476.

Stetter M., Müller A. and Lang E. W. (1994), Neural network model for the coordinated formation of orientation preference and orientation selectivity maps. Phys. Rev. E **50**, 4167–4181.

Stetter M., Kussinger M., Schels A., Seeger E. and Lang E. W. (1995), Self-organization of cortical receptive fields and columnar structures in a Hebb-trained neural network. Lecture Notes in Computer Science **930**, 37–44.

Swindale N. V. (1996), The development of topography in the visual cortex: review of models. Network **7**, 161–247.
Swindale N. V. (1998), Orientation tuning curves: empirical description and estimation of parameters. Biol. Cybern. **78**, 45–56.
Periodic-pattern-selective cells in monkey visual cortex. J. Neurosci. **12**, 1416–1434.
Weliky M. and Katz L. C. (1997), Disruption of orientation tuning in visual cortex by artificially correlated neuronal activity. Nature **386**, 680–685.
Wong R. O. L. and Oakley D. M. (1996), Changing patterns of spontaneous bursting activity of on and off ganglion cells during development. Neuron. **16**, 1087–1095.
Wong R. O. L. (1999), Retinal waves and visual system development. Annu. Rev. Neurosci. **22**, 29–47.